IOPscience iopscience.iop.org

Home Search Collections Journals About Contact us My IOPscience

Investigation of optical transitions in superlattices using photovoltage spectra

This article has been downloaded from IOPscience. Please scroll down to see the full text article.

1995 J. Phys.: Condens. Matter 7 9693

(http://iopscience.iop.org/0953-8984/7/49/030)

View the table of contents for this issue, or go to the journal homepage for more

Download details:
IP Address: 171.66.16.151
The article was downloaded on 12/05/2010 at 22:42

Please note that terms and conditions apply.

J. Phys.: Condens. Matter 7 (1995) 9693–9701. Printed in the UK

Investigation of optical transitions in superlattices using photovoltage spectra

Wenzhang Zhu†, Qihua Shen‡ and Shiyi Liu‡

† Jimei Navigation Institute, Xiamen, Fujian 361021, People's Republic of China
‡ Department of Physics, Xiamen University, Xiamen, Fujian 361005, People's Republic of China

Received 7 December 1994, in final form 22 August 1995

Abstract. This paper presents the experimental set-up and the measurement procedures of the photovoltage technique and reports a photovoltage spectroscopy study of the subband structures and the optical transitions in AlAs/GaAs superlattices at different temperatures ranging from 18 to 300 K. Below 100 K, the photovoltage spectra reflect the step-like distribution of the two-dimensional state density, and a sequence of distinct exciton transition peaks have been observed. The peaks are identified according to the selection rule of optical transitions and the calculated results. The experiments show that the photovoltage changes considerably with temperature. The mechanisms for the photovoltaic effect of superlattice and quantum well structures are given and the changes in photovoltage with temperature are discussed.

1. Introduction

There has been considerable interest in the novel optical properties and device applications of semiconductor superlattices and quantum well structures [1–3]. Optical transitions between conduction- and valence-band subbands in superlattices and quantum wells have been studied using a variety of different techniques, such as optical absorption [4], photoreflectance [5], photoluminescence [6] and photocurrent [7, 8]. However, no report has so far been made on the exciton transitions and the subband structures using the photovoltage method. The photovoltage spectrum not only reflects the ability of spectrum response of superlattices and quantum wells, which is of great importance, for example, in photoelectric device applications, but also provides information about subband structures, optical transitions and transports of photogenerated carriers. Collins *et al* [7] and Yamanaka *et al* [8] have observed a sequence of distinct exciton transition peaks, including allowed and forbidden transitions, in photocurrent spectra with extremely small light intensities, which demonstrates that photocurrent spectroscopy is a very sensitive technique for studying electronic structures of superlattices and quantum wells. In comparison with the photocurrent technique, in addition to the high sensitivity, the photovoltage technique presented in this paper has some advantages, including no damage to the sample and not having to make electrodes on the sample. In this paper, we describe the experimental set-up and the measurement procedures of the photovoltage technique and report a photovoltage spectroscopy study of the subband structures and the optical transitions of p^+–i–n^+ photodiodes in which the intrinsic regions were composed of AlAs/GaAs superlattices at different temperatures ranging from 18 to 300 K. As a means of non-destructive testing, the photovoltage technique is particularly suitable for testing the quality of crystal semiconductor

0953-8984/95/499693+09$19.50 © 1995 IOP Publishing Ltd

and epitaxy layers including the grown quality of superlattices and quantum wells and for monitoring the influence of the manufacturing process on the properties of semiconductor devices.

2. Experimental details

The two samples which will be discussed were grown by molecular-beam epitaxy (MBE). In each case the substrate is n^+-GaAs doped with Si at approximately 2×10^{18} cm^{-3}. On the substrate an undoped superlattice was grown. In sample 1 the superlattice consisted of 100 periods of 10 nm GaAs wells and 10 nm AlAs barriers. In sample 2 the superlattice consisted of 30 periods of 10 nm GaAs wells and 3 nm AlAs barriers. A p^+-AlAs layer which was about 10 nm thick and doped with Be at 5×10^{18} cm^{-3} was grown on top of the superlattice, followed by a p^+-GaAs cap layer about 10 nm thick and doped with Be at 5×10^{18} cm^{-3}. The resultant structure is a p^+–i–n^+ photodiode. This structure is schematically shown in figure 1.

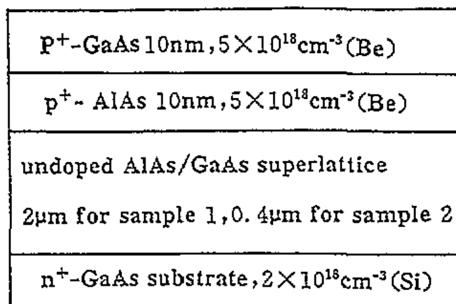

Figure 1. Schematic diagram of the AlAs/GaAs superlattice p^+–i–n^+ structure. The superlattice intrinsic region is composed of AlAs(10 nm)/GaAs(10 nm), 100 periods, for sample 1 and AlAs(3 nm)/GaAs(10 nm), 30 periods, for sample 2.

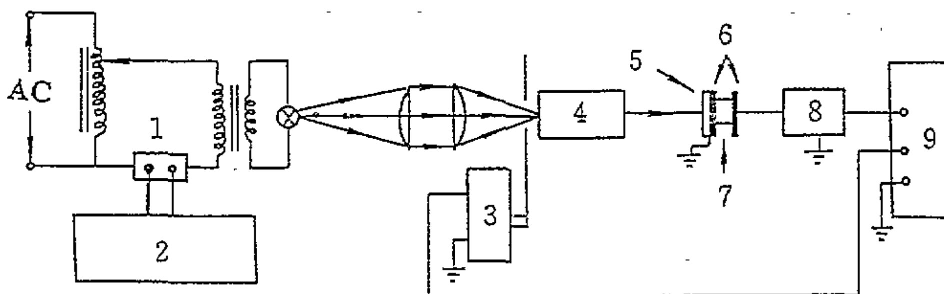

Figure 2. Schematic diagram of the experimental set-up for photovoltage spectrum measurement: 1, standard resistor; 2, digital AC voltmeter; 3, chopper; 4, grating monochromator; 5, conducting glass; 6, sheet mica; 7, sample; 8, electrostatic tube amplifier; 9, lock-in amplifier.

The diagram of the experimental set-up for measuring the photovoltage spectrum is shown in figure 2. The sample is mounted in a variable-temperature cryostat. The temperature is controlled with a thermoelectric couple controller. Light from a bromine tungsten lamp passes through a chopper, becoming a rectangular light pulse, and then is

focused onto a grating monochromator. The light chopper operates at about 20 Hz or at a frequency that is low enough to permit a steady-state distribution of carriers in the sample and high enough to permit effective capacitive coupling of the photovoltage signal into an amplifier. The resolution of the grating monochromator is 0.1 Å. The sample is illuminated on the front face with the monochromatic light pulse from the monochromator. When the photon energy of the incident light is greater than the band gap of the well material, electron–hole pairs are produced by band-to-band transitions and then separated by some mechanism to produce a photovoltage. The photovoltage signal is capacitively coupled by a transparent conducting glass and two pieces of sheet mica into an electrostatic tube amplifier for transformation of impedance and then is sent into a lock-in amplifier for measurement. The input impedance of the lock-in amplifier is 100 MΩ to match the high source impedance. The photovoltage signal from the lock-in amplifier is recorded as a function of the wavelength of the incident light by an IBM-386 microcomputer and the photovoltage spectrum is obtained.

The wavelength dependence of the intensity of the light source has been taken into account. In order to ensure the the intensity of the incident photon flux at different wavelengths is the same, a linear thermoelectric pile was used to perform calibration of equal photon fluxes. The output voltage of the linear thermoelectric pile is proportional to the photon flux density, or

$$V = gN_p h\nu = gN_p hc/\lambda \tag{1}$$

where N_p is the number of photons illuminated on the thermoelectric pile per second, h is Planck's constant, c is the light velocity and λ is the wavelength of incident light. The proportionality factor g expresses the sensitivity of the thermoelectric pile and $g = 0.43$ V W^{-1} cm^2 for the thermoelectric pile used here. Suppose that the output voltages of the thermoelectic pile are V_1 and V_2, respectively, for the incident wavelengths λ_1 and λ_2. From equation (1), we obtain

$$V_1/V_2 = N_1\lambda_2/N_2\lambda_1. \tag{2}$$

Under the condition of equal photon fluxes, $N_1 = N_2$, equation (2) reduces to

$$V_1/V_2 = \lambda_2/\lambda_1. \tag{3}$$

The measurement system is calibrated in accordance with equation (3).

3. Results and analysis

The photovoltage spectra of AlAs/GaAs superlattices were measured at eight different temperatures: 18 K, 40 K, 70 K, 100 K, 150 K, 200 K, 250 K and 300 K. Typical photovoltage spectra are presented in figures 3 and 4.

(i) Figure 3 shows the photovoltage spectra for sample 1 at different temperatures. Six exciton peaks, labelled 11H, 11L, 13H, 31H, 33H and 33L have been observed (where ijH (ijL) is the exciton associated with the $n = i$ conduction-band subband and the $n = j$ heavy-hole (light-hole) valence-band subband). However, 22H and 22L exciton transitions have not been observed. Figure 4 shows the photovoltage spectra for sample 2 at different temperatures. Six peaks labelled 11H, 11L, 22H, 22L, 33H and 33L have been observed. The peaks are identified according to the selection rule of optical transition and the calculated results. We adopted the new formalism of the Kronig–Penney model [9] with Bastard's [10] boundary condition to calculate the energy levels of the conduction-band subbands and valence-band subbands. We have taken [11, 12] $\Delta E_c : \Delta E_v = 60\% : 40\%$ as the

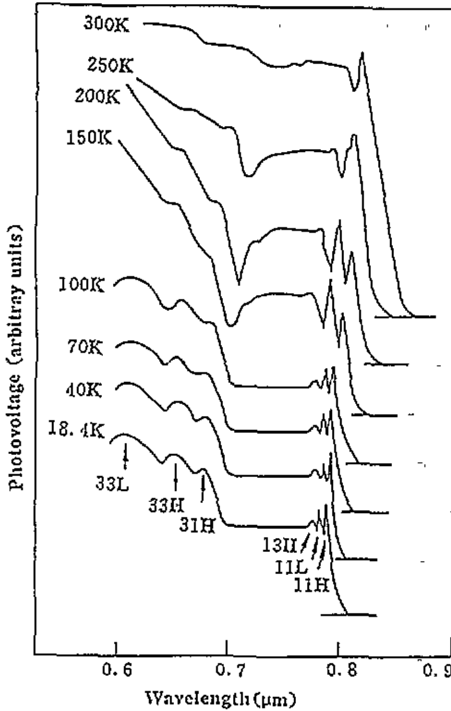

Figure 3. Photovoltage spectra for sample 1 at different temperatures. The temperature is given to the left of each spectrum. The exciton peaks have been labelled in the figure. In this sample the GaAs well and AlAs barrier are both 10 nm thick, 100 periods.

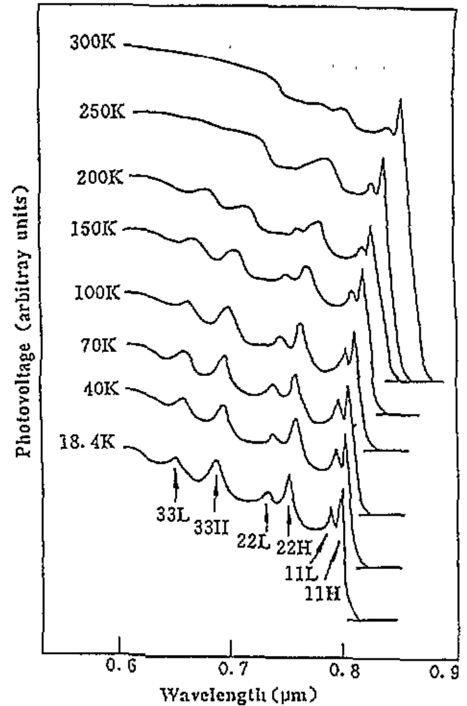

Figure 4. Photovoltage spectra for sample 2 at different temperatures. The temperature is given to the left of each spectrum. The exciton peaks have been labelled in the figure. In this sample the GaAs well is 10 nm thick and the AlAs barrier is 3 nm thick, 30 periods.

band offset ratio. The effective masses used are [11, 13] $m_{e1} = 0.0665m_0$, $m_{H1} = 0.34m_0$ and $m_{L1} = 0.094m_0$ for GaAs at the well layers and $m_{e2} = 0.15m_0$, $m_{H2} = 0.76m_0$ and $m_{L2} = 0.15m_0$ for AlAs at the barrier layers, where m_0 is the free-electron mass. Some calculated energies of the intrinsic exciton transitions at 18.4 K are listed in table 1. The energies of the observed peak positions are also listed in table 1. From table 1, we can see that the calculated results are in agreement with experiments.

(ii) Figure 3 shows that the photovoltage steeply drops at about 1.75 eV at a temperature of 150–250 K for sample 1. The drop was observed in only a few samples and was found to be related to the etching treatment of the surface of the sample. It is suggested that strong absorption which makes no contribution to the photovoltage exists in the surface layer of sample 1. The strong absorption may results from the surface defects. The incident light is absorbed strongly in the surface layer, but the photogenerated carriers in the surface layer recombine quickly for high-surface recombination velocity and make no contribution to the photovoltage. However, the precise mechanism is unclear at present. The value of 1.75 eV is in agreement with the energy of $n = 2$ exciton transitions, which accounts for the fact that 22H and 22L exciton transitions have not been observed in sample 1.

(iii) Figures 5 and 6 are plots of photovoltage as a function of temperature at four excitation wavelengths 0.78, 0.75, 0.72 and 0.68 μm, for samples 1 and 2, respectively. The experimental results show that the photovoltage changes considerably with temperature.

Table 1. The experimental and theoretical values of the energies of exciton transitions in two superlattices AlAs(10 nm)/GaAs(10 nm) (sample 1) and AlAs(3 nm)/GaAs(10 nm) (sample 2) at 18.4 K. The experimental values are the peak positions observed in photovoltage spectra. The theoretical values are the results calculated by the Kronig–Penney model with Bastard's boundary conditions.

	Energy (eV) of the following exciton transitions							
	11H	11L	22H	22L	13H	31H	33H	33L
Sample 1, experiment	1.560	1.575	—	—	1.598	1.817	1.879	2.008
Sample 1, theory	1.558	1.574	1.679	1.742	1.601	1.819	1.883	2.020
Sample 2, experiment	1.554	1.567	1.651	1.701	—	—	1.805	1.913
Sample 2, theory	1.549	1.560	1.643	1.691	1.598	1.749	1.789	1.901

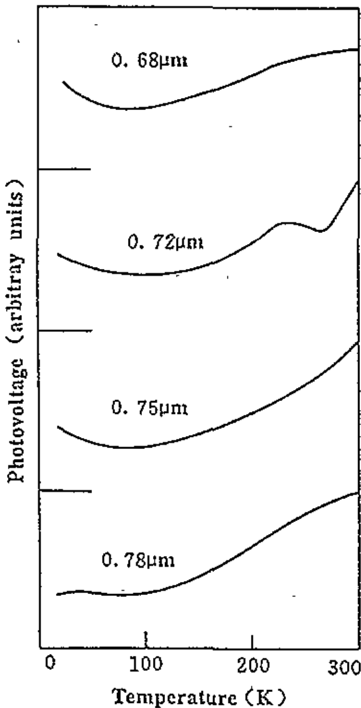

Figure 5. Photovoltage as a function of temperature at four excitation wavelengths for sample 1. The *excitation wavelength is given for each curve.*

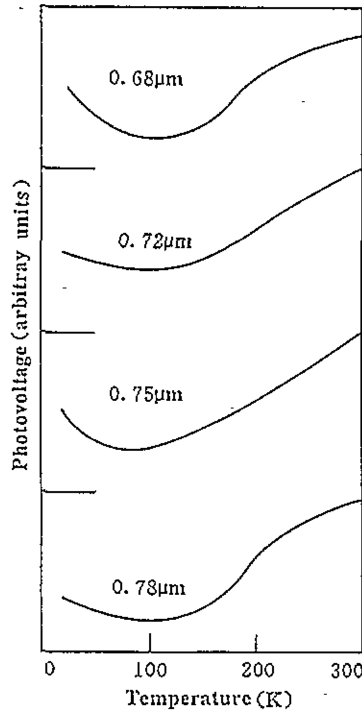

Figure 6. Photovoltage as a function of temperature at four excitation wavelengths for sample 2. The *excitation wavelength is given for each curve.*

As the features in the photovoltage spectra observed shift with the temperature, the change in photovoltage with temperature is a complex effect: the temperature dependence of a particular feature and the temperature shift of the spectrum. The change in the photovoltage amplitude that results from the shift of the photovoltage spectrum with temperature is gentle except around the peaks, which can be seen from figures 3 and 4. Therefore, the change in the photovoltage with temperature mainly results from the temperature dependence of the features. The plots of photovoltage as a function of temperature in figures 5 and 6

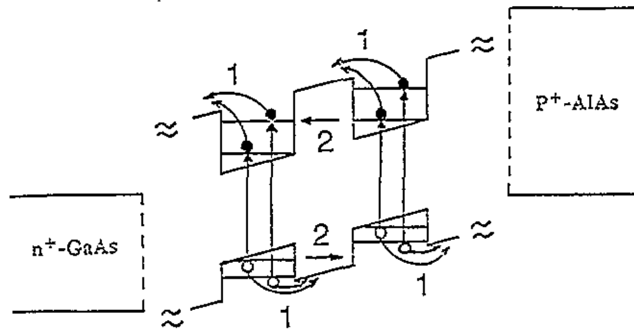

Figure 7. Energy-band diagram of the p^+–i–n^+ heterostructure in figure 1 and transport processes of photogenerated carriers. Process 1 shows the photogenerated carriers across barriers by thermionic emission and process 2 shows the tunnel effect.

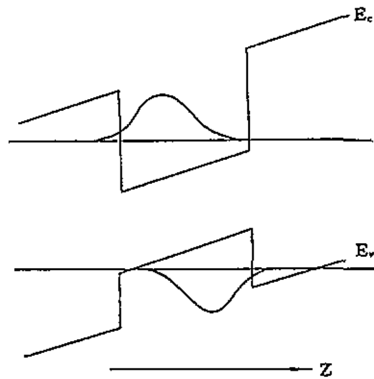

Figure 8. Spatial separation effect of the photogenerated electrons and holes in the GaAs wells of the AlAs/GaAs superlattice.

approximately express the temperature dependence of the features. It can be seen from figures 5 and 6 that for a given excitation wavelength the photovoltage decreases as the temperature of the sample is decreased from 300 K to a critical temperature T_c and slightly increases as the temperature is further lowered. The experiments show that the critical temperature T_c is different for samples with different structures and is in the range 80–110 K for all the samples that we studied. For the sample with the wider barrier, T_c is lower. T_c is about 90 K for sample 1 and 110 K for sample 2. The reason for the dependence of the photovoltage on temperature is that the transport mechanisms which play the main role in the transport process of the photogenerated carriers are different at different temperatures. In our view, the photovoltage of the AlAs/GaAs superlattice and quantum well structures comes from three kinds of photovoltaic effect.

(1) The photovoltage V_E results from the photogenerated carriers separated by the p^+–i–n^+ built-in electric field and then across barriers by thermionic emission, as process 1 shown in figure 7. The photogenerated holes move towards the front face (p^+ region) and the photogenerated electrons move towards the back face (n^+ region). This photovoltaic effect becomes stronger at higher temperatures. This photovoltaic effect is an important mechanism for quantum well structures.

(2) The photovoltage V_T results from the photogenerated carriers across barriers by the

tunnel effect, as process 2 shown in figure 7. This photovoltaic effect is the main mechanism in superlattices.

(3) The photovoltage V_s results from the spatial separation effect of the photogenerated carriers. What the spatial separation effect means is that, in a superlattice with thick barriers or in a quantum well structure, the probability that photogenerated carriers tunnel through barriers is small and so the photogenerated electrons and holes separated by the built-in electric field of the p^+–i–n^+ junction are still confined in the wells by the barriers, as shown in figure 8.

The system may be considered as a series of capacitors corresponding to each period with the positive plate located at the z mean value of the hole wavefunction Z_h, and the negative plate at the z mean value of the electron wavefunction Z_e. The potential difference V_s across the superlattice is equal to the sum of local potential differences ΔV_i between the planes Z_{hi} and Z_{ei} limiting the ith period and is given by $V_s = \sum_{i=1}^{N} \Delta V_i$ for an N-period superlattice or quantum well structure. This photovoltaic effect becomes stronger at lower temperatures.

The number of carriers across the barrier due to thermionic emission is proportional to [14, 15] $\exp(-q\Delta E/k_B T)$, where ΔE is the potential energy. Thus, for a small photovoltage signal (less than $k_B T/q$), the photovoltage that comes from the first kind of photovoltaic effect is given by

$$V_E \propto \exp(-q\Delta E/k_B T). \tag{4}$$

The tunnelling probability for a square barrier is proportional to [16] $\exp(-\beta\Delta E^{1/2}b)$, where β is a constant and b is the width of the barrier. Thus, for a small photovoltage signal (less than $k_B T/q$), the photovoltage that comes from the second kind of photovoltaic effect is given by

$$V_T \propto \exp(-\beta\Delta E^{1/2}b). \tag{5}$$

The photovoltage comes from the third photovoltaic effect—spatial separation of electrons and holes—and is given by

$$V_S = \sum_{i=1}^{N} \Delta V_i = \sum_{i=1}^{N} \frac{Q_i}{C} = \frac{Z_h - Z_e}{\epsilon_r \epsilon_0 S} \sum_{i=1}^{N} Q_i \tag{6}$$

where N is the number of periods of a superlattice or quantum well structure, S is the sample area, $Z_h - Z_e$ is the separation of the two charge packets, Q_i is the total charge of photogenerated electrons or photo-generated holes in the ith well, ϵ_r is the relative dielectric constant and ϵ_0 is the permittivity in vacuum. In the interesting optical waveband (E_g (GaAs well) $\leqslant h\nu \leqslant E_g$ (AlAs barrier)), optical absorption takes place only in the GaAs wells. Neglecting the absorption in the cap layer, the hole–electron generation rate G is given by

$$G(z) = I_0(1 - R)\eta\alpha \exp(-\alpha z) \tag{7}$$

where I_0 is the incident photon flux per unit area, R is the reflection coefficient, η is the quantum efficiency, α is the absorption coefficient of GaAs wells and z is the total thickness of the GaAs wells through which the light passed.

The photogenerated carrier density n_{ph} in the GaAs wells obeys the following rate equation:

$$\frac{\mathrm{d}n_{ph}}{\mathrm{d}t} = G - \frac{n_{ph}}{\tau} \tag{8}$$

where τ is the lifetime of photogenerated carriers.

As the frequency of the light pulse is low enough to permit a steady-state distribution of carriers, we consider the case when $\mathrm{d}n_{ph}/\mathrm{d}t = 0$. The photogenerated carrier density n_{ph} can be obtained from equation (8):

$$n_{ph} = G\tau. \tag{9}$$

The total charge of the photogenerated electrons or holes is given by

$$\begin{aligned}\sum_{i=1}^{N} Q_i &= qS\int_0^{Na} n_{ph}\,\mathrm{d}z = qS\tau\int_0^{Na} G(z)\,\mathrm{d}z \\ &= qS\tau I_0(1-R)\eta[1-\exp(-N\alpha a)]\end{aligned} \tag{10}$$

where q is the elementary charge and a is the width of the GaAs well.

Substituting equation (10) into equation (6) yields

$$V_s = q\tau I_0(1-R)\eta[1-\exp(-N\alpha a)]\frac{Z_h - Z_e}{\epsilon_r\epsilon_0}. \tag{11}$$

Since the thermal motion of the carriers becomes more violent as the temperature rises, $Z_h - Z_e$ becomes smaller at higher temperatures. However, the exact dependence of V_s on the temperature is not completely understood at present.

From figures 5 and 6 and equations (4), (5) and (11), we come to the conclusion that the photovoltage mainly comes from the first kind of photovoltaic effect in the temperature range from 300 K to T_c, and from the second and third kinds of photovoltaic effect at temperatures below T_c. At temperatures below T_c, the tunnel effect plays the main role in the sample with thin barriers, and the spatial separation effect plays the main role in the sample with thick barriers.

(4) At temperatures below 100 K, the photovoltage increases in a step-like manner with decreasing wavelength of incident light, which reflects the step-like distribution of the two-dimensional state density in superlattice. The nth plateau corresponds to the transition from the nth valence subband to the nth conduction subband. On condition that there is no loss of photogenerated carriers, the photovoltage V_{ph} is proportional to the optical absorption, which is proportional to the joint density ρ_{cv} of states. So V_{ph} is proportional to ρ_{cv}.

4. Conclusion

Because of its simplicity and high sensitivity, photovoltage spectroscopy is an effective technique for studies of the electronic properties of superlattices and quantum well structures. At temperatures below 100 K, the photovoltage spectrum reflects the step-like distribution of the two-dimensional state density in superlattice. Eight intrinsic exciton transitions, including two forbidden transitions 13H and 31H, have been observed. The photovoltage mainly comes from the photogenerated carriers across barriers by thermionic emission at temperatures above T_c and from the spatial separated effect and tunnelling effect of the photogenerated carriers at temperatures below T_c.

References

[1] Mendez E E, Chang L L, Landgen G, Ludeke R and Esaki L 1981 *Phys. Rev. Lett.* **46** 1230
[2] Schmitt-Rink S, Chemla D S and Miller D A B 1989 *Adv. Phys.* **38** 89
[3] Miller R C and Kleinman D A 1985 *J. Lumin.* **30** 520
[4] Masselink W T, Poarah P J, Klem J, Peng C K, Morkoc H, Sanders G D and Chang Y C 1985 *Phys. Rev.* B **32** 8027

[5] Glembocki O J, Shanabrook B V, Bottka N, Beard W T and Comas J 1985 *Appl. Phys. Lett.* **46** 920
[6] Miller R C, Gossand A C, Sanders G D and Chang Y C 1985 *Phys. Rev.* B **32** 8452
[7] Collins R T, Klitzing K V and Ploog K 1986 *Phys. Rev.* B **33** 4378
[8] Yamanaka K, Fukunaka T, Tsukada N, Kobayashi K L I and Ishii M 1986 *Appl. Phys. Lett.* **48** 840
[9] Cho H S and Prucnal P R 1987 *Phys. Rev.* B **36** 3237
[10] Bastard G 1981 *Phys. Rev.* B **24** 5693
[11] Miller R C, Kleinman D A and Gossard A C 1984 *Phys. Rev.* B **29** 7085
[12] Sanders G D and Chang Y C 1985 *Phys. Rev.* B **32** 5517
[13] Adachi S 1985 *J. Appl. Phys.* **58** R1
[14] Anderson R L 1962 *Solid-State Electron.* **5** 341
[15] Perlman S S and Feucht D L 1964 *Solid State Electron.* **7** 911
[16] Kane E O 1961 *J. Appl. Phys.* **32** 83